Antibacterial and Cellular Response of Hydroxyapatite (HA) and HA- x ZnO (x = 3.0,

4.5, and 7.5 wt. %) Composites

This chapter discusses the effect of incorporation of varying amount of ZnO (0.0, 3.0, 4.5 and 7.5 wt. %) in HA matrix on antibacterial and cellular response. The phase evolution, FTIR and microstructural analyses of fabricated HA- x ZnO (0.0, 3.0, 4.5 and 7.5 wt. %) composites have been discussed. Further, the effect of addition of ZnO on dielectric and electrical properties has been discussed. In addition, the combined effect of surface polarization and optimal ZnO addition in HA on antibacterial as well as cellular response has also been explored.

4.1. XRD analysis

Fig. 4.1 represents the x-ray diffraction patterns for HA and HA-x ZnO (x=3, 4.5 and 7.5 wt. %) composites. The major diffraction peaks of HA is observed at, $2\theta = 31.86°$, $32.28°$, $32.98°$ and $34.12°$. These values correspond to the single phase hexagonal HA structure (JCPDS # 09-0432). On the other hand, the diffraction peaks corresponding to ZnO appears at $2\theta = 31.83°$, $36.36°$, and $56.62°$, which is similar to the XRD pattern of wurtzite hexagonal ZnO (JCPDS # 79-2205). In the composite samples, the diffraction peaks, corresponding to only HA and ZnO phases were observed which represents the thermochemical stability of HA-ZnO composites under the optimal processing parameters.
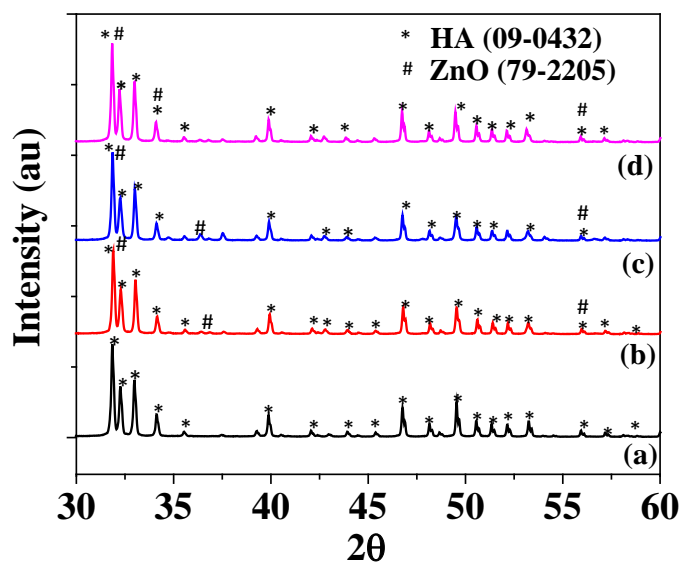
Fig. 4.1. The X- ray diffraction patterns for (a) HA, (b) HA-3.0 wt. % ZnO, (c) HA-4.5 wt. % ZnO and (d) HA-7.5 wt. % ZnO composite samples.

4.2. Fourier transform infrared spectroscopic analysis

Fig. 4.2. illustrates the FTIR spectra of sintered HA-x ZnO (x = 0.0, 3.0, 4.5 and 7.5 wt. % ZnO) composites. The characteristic bands, corresponding to PO_4^{3-} in HA appears at 1089, 1023, 962, 604, and 560 cm^{-1}[1]. The adsorption bands, corresponding to CO_3^{2-} appears at 1415 and 1450 cm^{-1} [2]. The band at 874 cm^{-1} represents the HPO_4^{2-} [3]. The stretching and bending modes of vibration, corresponding to hydroxyl group (OH⁻), are observed at 3572 and 630 cm^{-1}, respectively [4].
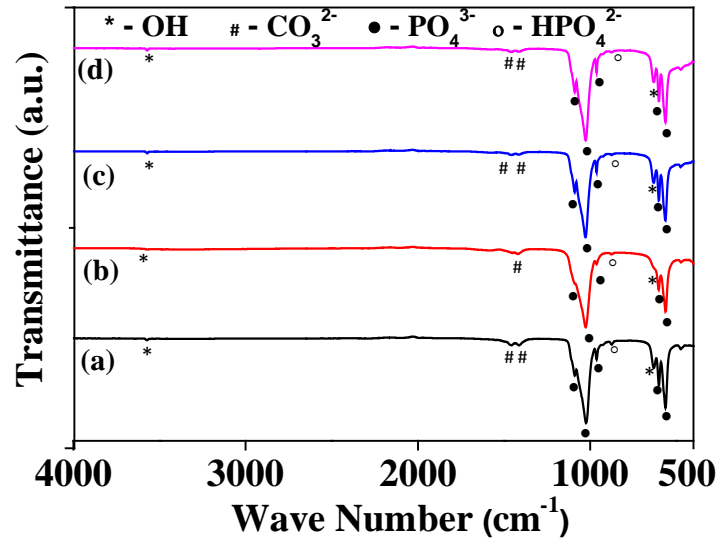
Fig. 4.2. Fourier transform infra-red (FTIR) spectra for (a) HA, (b) HA-3.0 wt. % ZnO, (c) HA-4.5 wt. % ZnO and (d) HA-7.5 wt. % ZnO composite samples.

4.3. Microstructural analysis

Fig. 4.3 represents the SEM images of fractured HA and HA-x ZnO (x = 3.0, 4.5, 7.5 wt. %) composite surfaces. The brittle mode of fracture has been observed in HA and composite samples. The average grain size of HA and HA-x ZnO (x = 3.0, 4.5, and 7.5 wt. %) composites were calculated to be $\pm$ 0.89, $\pm$ 0.96, $\pm$ 0.99 and $\pm$ 1.28 µm, respectively. The energy dispersive X-ray (EDX) analyses confirm the presence of ZnO in the composite samples. The fractured surfaces reveal good densification of the sample at the optimal processing parameter.
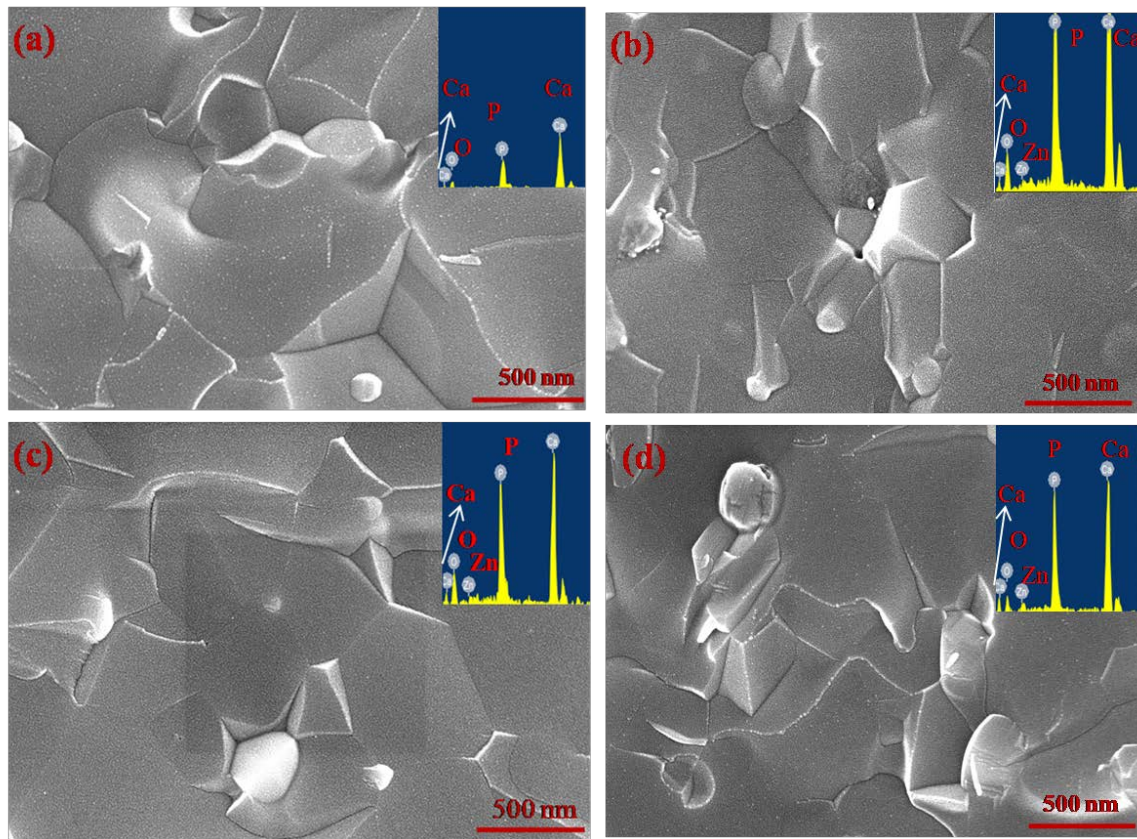
Fig. 4.3. Scanning electron micrographs of fractured (a) HA, (b) HA-3.0 wt. % ZnO, (c) HA-4.5 wt. % ZnO and (d) HA-7.5 wt. % ZnO composite surfaces.

4.4. Dielectric measurements

The dielectric and electrical measurements of pure HA as well as the composites were performed using Alpha-A High-Performance Frequency Analyzer, in the temperature and frequency range of 30- 500ºC and 0.1Hz-1MHz, respectively. For dielectric measurements, 10 mm diameter and 1.5 mm thickness pellets were prepared. The samples were mirror polished and electroded using Ag paste, which were then cured at 700ºC for 5 min.

The AC conductivity of HA and HA-ZnO composites were calculated with the help of recorded data for dielectric measurement using the equation (4.1) [5],

$$\sigma_{ac} = \omega C \frac{d}{A} \tan \delta \qquad (4.1)$$

Where, ω is angular frequency ($\omega = 2\pi f$), $\tan \delta$ is dielectric loss, C, d and A are capacitance, thickness and area of the samples, respectively.

4.4.1. Dielectric behavior

The dielectric response of HA and HA-xZnO (x = 3.0, 4.5, 7.5 wt. %) composites in the temperature range of 35 to 500 ℃ at a few selected frequencies are represented in Fig. 4.4. The dielectric constant of HA [Fig. 4.4 (a)] is observed to be poorly dependent on temperature up to 200 ℃. However, the dielectric constant increases with temperature in the high temperature region (> 200 ℃). The dielectric loss curve shows almost similar behavior. In case of HA-3 ZnO composite, diffused maxima at about 100 ℃ [Fig. 4.4 (b)] and another in the higher temperature (350- 400 ℃) region can be seen. For HA-x ZnO (x = 4.5 and 7.5 wt. % ZnO) composites, almost temperature independent dielectric constant [Fig. 4.4 (c and d)] has been observed up to ~ 250 ℃, which is followed by peak with further increase in temperature. The peak observed at about 400 ℃ represents the dynamic stabilization of hexagonal phase due to reorientation of OH$^-$ ions [6]. The dielectric loss of HA-x ZnO composites shows the similar behavior to that of dielectric constant. The dielectric behavior of HA at lower temperature (< 100 ℃) depends upon the processing based structural defects such as, OH$^-$ and O$^-$ ions, and vacancies [7]. However, at higher temperature (> 500 ℃), migration of OH$^-$ ions are responsible for conduction [8].
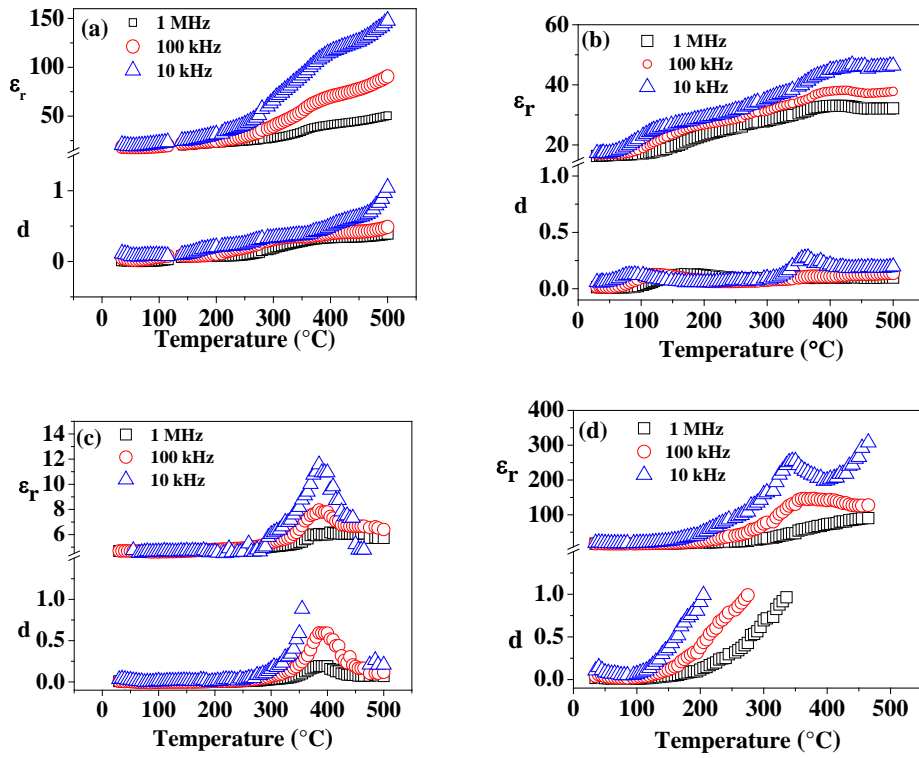
Fig. 4.4. Variation of dielectric constant and loss with temperature for (a) HA, (b) HA-3.0 wt. % ZnO, (c) HA- 4.5 wt. % ZnO and (d) HA- 7.5 wt. % ZnO at few selected frequencies.

The phase transformation of HA, from monoclinic to hexagonal occurs at 210ºC, because of the orientation of OH⁻ ions [9]. Above 300ºC, thermal defects and hydroxylation of HA [Eq. (4.2)] are responsible for the observed dielectric response [10].

$$\mathbf{Ca_9(HPO_4)(PO_4)_5(OH) = 3Ca_3(PO_4)_2 + H_2O} \qquad (4.2)$$

Oxygen in form of O_2^- and O^- ions are adsorbed on the surface of ZnO at lower temperature. However, with increasing the temperature, the rate of release of adsorbed oxygen increases [11]. Consequently, a large number of oxygen vacancies are formed, these oxygen vacancies are accumulated with grain boundary and increase the polarization at higher temperature [12]. The room temperature dielectric constant and

91

loss values for HA, HA-3 ZnO, HA-4.5 ZnO and HA-7.5 ZnO composites are (17.9, 0.11), (16.3, 0.53), (4.6, 0.04) and (17, 0.11), respectively, measured at a frequency of 10 kHz. The dielectric constant of ZnO has been reported to be 8.5 at room temperature and frequency of 10 kHz [13]. The dielectric constant of natural human bone has been suggested to be around 10 [14]. The measured values of the dielectric constant have been compared with those of the calculated from existing theoretical models. The dielectric constant values for HA-3.0 ZnO, HA-4.5 ZnO and HA- 7.5 ZnO composites were calculated using parallel and series Wiener bounds [Eqs. (4.3) and (4.4)] as well as logarithmic mixture rule [Eq. (4.5)] as [15],

$$\varepsilon_{composite} = V_{HA}\varepsilon_{HA} + V_{ZnO}\varepsilon_{ZnO} \qquad (4.3)$$

$$\frac{1}{\varepsilon_{composite}} = \frac{V_{HA}}{\varepsilon_{HA}} + \frac{V_{ZnO}}{\varepsilon_{ZnO}} \qquad (4.4)$$

$$\log_{\varepsilon_{composite}} = V_{HA}\log\varepsilon_{HA} + V_{ZnO}\log\varepsilon_{ZnO} \qquad (4.5)$$

Where, ε and V is the dielectric constant and volume fraction, respectively.

It is clearly observed from Fig. 4.5 that the experimental values of dielectric constant for HA-x ZnO composites are lower than those, calculated using the Eqs. (4.3), (4.4) and (4.5) at room temperature and frequency of 10 kHz. The connectivity between HA and secondary phase (ZnO) can be one of the reasons for such deviation in dielectric constant values. The small amount of ZnO in HA results in 0-3 connectivity between ZnO and HA phases in HA-ZnO composite.

The Landaure's expression for 0-3 connectivity for binary system is given as [16],

$$F = V_1 \frac{\varepsilon_1 - \varepsilon_c}{\varepsilon_1 + 2\varepsilon_c} + V_2 \frac{\varepsilon_2 - \varepsilon_c}{\varepsilon_2 + 2\varepsilon_c} \qquad (4.6)$$

Where, V1 and V2 are the volume fractions of constituent phases, ε_1 ε_2 and ε_c are the dielectric constants of ZnO, HA and composite, respectively. For perfect 0-3 connectivity, F should be zero. The value of F for HA-3.0 ZnO, HA-4.5 ZnO and HA-7.5 ZnO composites is calculated [Eq. 4.6] to be 0.027, 0.49, and 0.078, respectively. The effective dielectric constant of polyphase materials can also be calculated by Maxwell-Garnet equations [17].

$$\varepsilon_{eff} = \frac{\varepsilon_{HA} V_{HA}[\frac{2}{3} + \frac{\varepsilon_{ZnO}}{3\varepsilon_{HA}}] + \varepsilon_{ZnO} V_{ZnO}}{V_{HA}[\frac{2}{3} + \frac{\varepsilon_{ZnO}}{3\varepsilon_{HA}}] + V_{ZnO}} \qquad (4.7)$$

The effective dielectric constant of HA- 3.0 ZnO, HA- 4.5 ZnO and HA- 7.5 ZnO composites were calculated using the above expression at the frequency of 10 kHz and room temperature are 17.1, 17.6 and 19.9, respectively. The measured value of dielectric constant for HA-x ZnO (x =3.0, 4.5 and 7.5 wt. % ZnO), composites deviated about 4.6 %, 72 % and 1.45 %, respectively, with those of the calculated [Eq. 4.7] values.
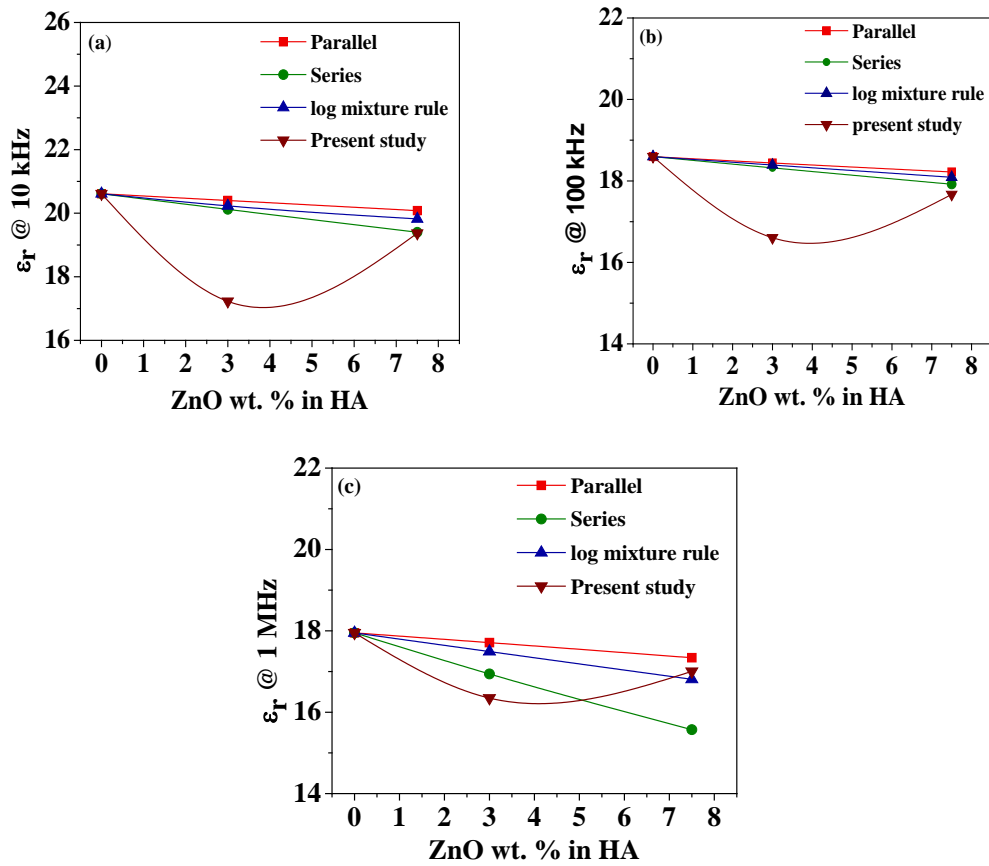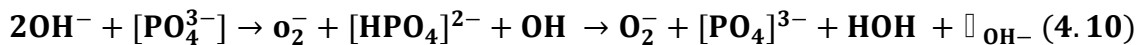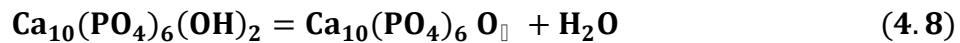
Fig. 4.5. Comparison of experimental values for HA-xZnO (x= 3.0,4.5 and 7.5 wt.%) with those of the values, obtained using theoretical models (Eqs. 4.5-4.7) at frequencies of (a) 10 kHz, (b) 100 kHz and (c) 1 MHz.

4.4.2. AC conductivity behavior

Fig. 4.6 represents the variation of ac conductivity with inverse of temperature at frequencies of 10 kHz, 100 kHz, and 1 MHz for HA and HA-ZnO composites. A diffused maximum in the temperature range of 100- 250ºC is observed for HA. However, for HA-3.0 ZnO and HA-7.5 ZnO composites, the maxima is observed in the temperature range of 60-200ºC and 60-120ºC, respectively. The sharp peaks [Fig. 4.6 (b, c), @ 10 kHz], is observed at about 400ºC, due to dielectric relaxation in the samples [18].

The diffused maxima shift towards higher temperature with increase in the frequency. The ac conductivity values for HA, HA-3.0 ZnO, HA-4.5 ZnO and HA-7.5 ZnO composites at room temperature and frequency of 10 kHz are 1.29×10^{-8}, 5.65×10^{-9}, 6.82×10^{-8} and 4.29×10^{-9} (ohm cm)$^{-1}$. For natural bone, ac conductivity has been reported to be in the range of 10^{-10} to 10^{-9} (ohm cm)$^{-1}$[19]. It has been suggested that the conduction of HA at lower temperature (< 100ºC), is due to the migration of protons (H$^+$) in adsorbed water [20]. However, at higher temperature (> 300ºC), dehydration of OH$^-$ ions are responsible for conduction [21]. The increase in conductivity at higher temperature is associated with the hopping of H$^+$ at O^{2-} sites [Eq. (4.8)] [22]. In HA, two proton conduction mechanisms have been suggested. Firstly, protons conduct via OH$^-$ sites along c-axis (Eq. 4.9). Another mechanism involves conduction of protons via PO$_4$$^{3-}$ tetrahedra [23]. The second mechanism is feasible due to comparatively shorter distance (0.307 nm) between the PO$_4$$^{3-}$ tetrahedra and OH$^-$ ions (Eq. 4.10) with that of adjacent OH- ions (0.344 nm) sites [24]. In addition, in first mechanism, conduction can be hindered by the defects at OH$^-$ sites which are created due to the dehydration of the lattice OH$^-$ ions along c-axis.

$$Ca_{10}(PO_4)_6(OH)_2 = Ca_{10}(PO_4)_6\, O_\square + H_2O \qquad (4.8)$$

$$OH^- + OH^- \rightarrow O^{2-} + HOH \qquad (4.9)$$

$$2OH^- + [PO_4^{3-}] \rightarrow o_2^- + [HPO_4]^{2-} + OH \rightarrow O_2^- + [PO_4]^{3-} + HOH + \square_{OH-} \quad (4.10)$$
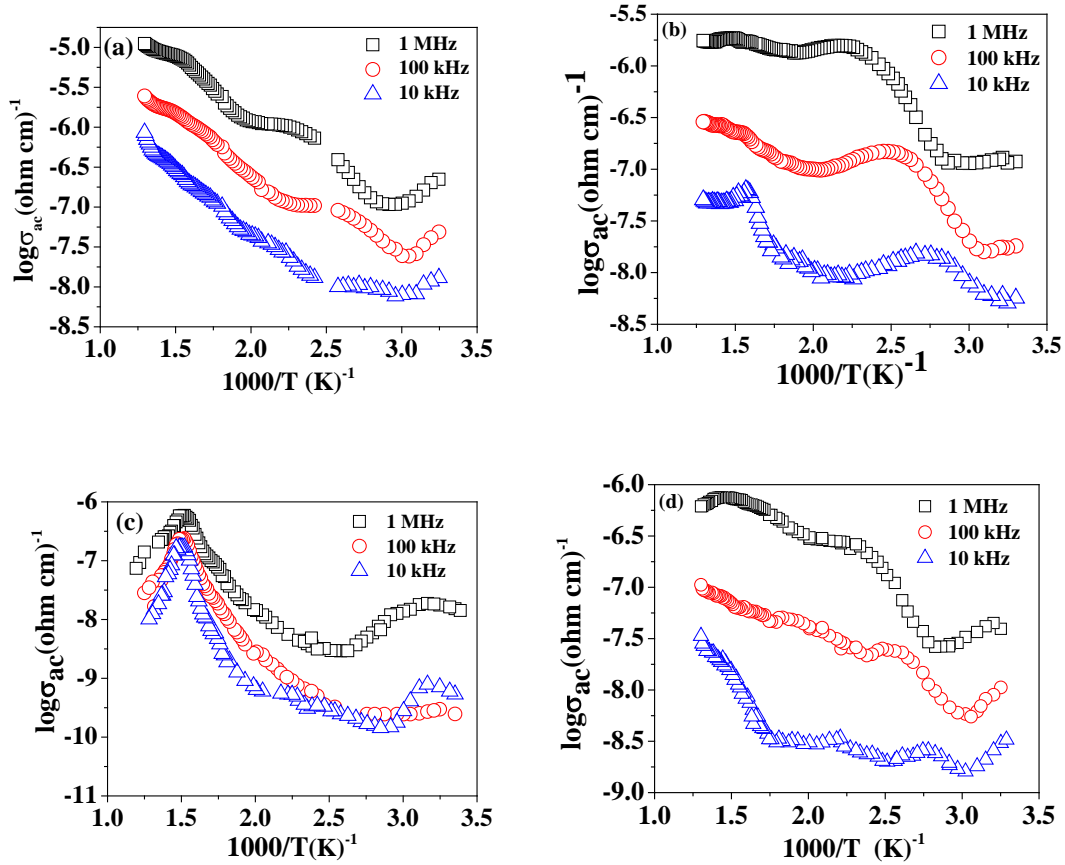
Where, $\square$ represents the vacancy.

Fig. 4.6. Variation of ac conductivity with inverse of temperature for compositions (a) HA, (b) HA-3.0 wt. % ZnO, (c) HA-4.5 wt. % ZnO and (d) HA-7.5 wt. % ZnO.

4.4.3. Impedance analysis

Fig. 4.7 represents the complex plane impedance response for HA and HA-3.0 ZnO composite. The impedance analyses were performed to understand the behavior of grain and grain boundary in the entire spectrum as a function of resistance and capacitance [25]. It is clearly observed from Fig. 4.7 (a, b) that the centers of semicircular arcs appear below the x-axis which shows the multiple relaxation processes i.e., non-Debye type relaxation in the samples [26]. The intercepts of semicircles on the real axis give information about the grain and grain boundary resistances [27].

In case of non-Debye type relaxation behavior, the constant phase element (CPE) explains the variation from Debye-type relaxation process [28]. The value of CPE were

calculated using the expression $C = (R^{1-n}C_Q)^{1/n}$, where, R and C_Q are the resistance and capacitance, respectively, used to define the CPE by varying n; n > 0 for non ideal case [29].The resistance and CPE are represented as parallel combination and each combination has a time constant to describe the relaxation behavior. The maxima in each semicircular arc are used to obtain the relaxation frequency of the circuit. The relaxation frequencies of grains and grain boundaries for HA have been calculated to be (8, 0.3 kHz), (1.9, 0.3 kHz), (22, 0.4 kHz), (52, 0.5 kHz) and (140, 0.4 kHz) at temperatures of 400,425, 450,475 and 500ºC, respectively. Similarly, for HA-3 ZnO composite, the relaxation frequencies of grains and grain boundaries have been calculated to be (41, 0.32 kHz), (18, 0.3 kHz), (20, 0.18 kHz), (8.1, 0.23 kHz) and (60, 0.84 kHz), respectively, at similar temperature. Fig. 4.7 (c, d) represents the plot of grain and grain boundary resistances (log R_g and log R_{gb}) with inverse of temperature for HA and HA-3.0 ZnO composite, respectively. The activation energies of both samples were calculated with the help of linear fitting of [log Rg /log R_{gb} Vs 1000/T] plot. For HA and HA-3.0 ZnO composite, the activation energies of grains and grain boundaries are (1.36, 1.44 eV), and (1.18, 1.98 eV), respectively. Yamashita et al. [30] reported the activation energy of HA to be 1.86 eV. The activation energy for H^+ and O_2^{2-} conduction has been reported to be 0.5 and 1.5 eV, respectively [31].
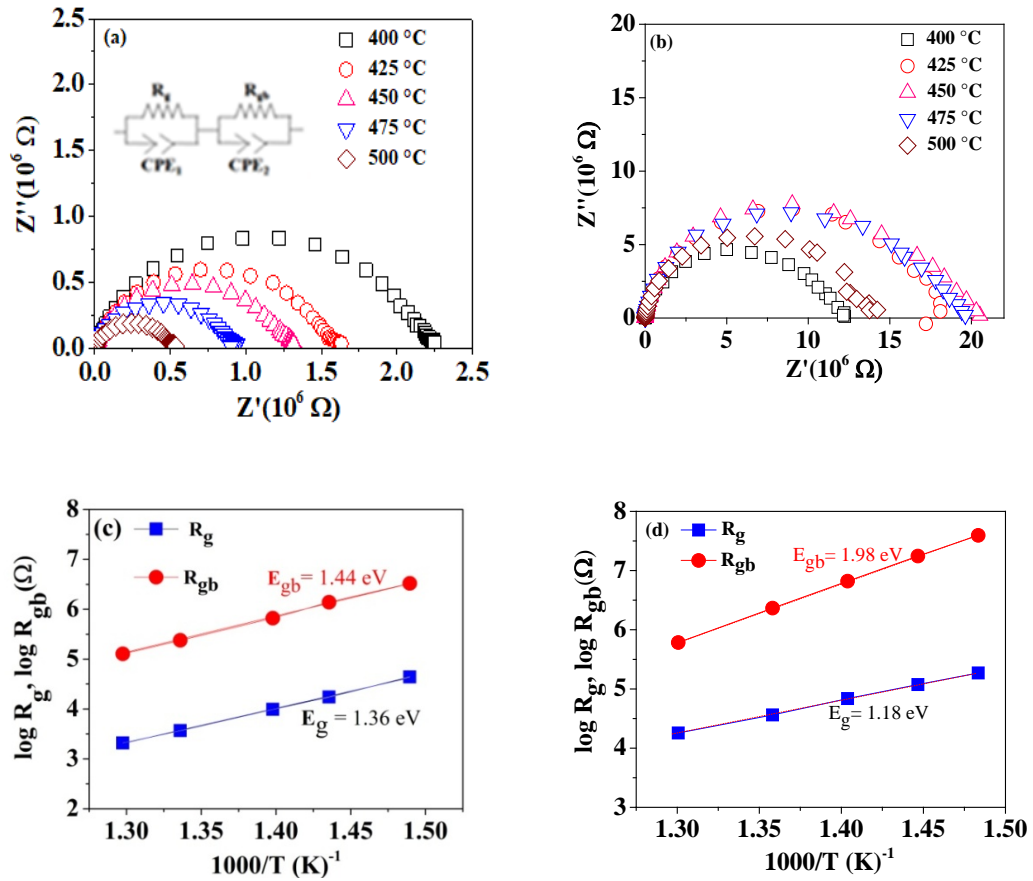
Fig. 4.7. Complex plane impedance plots for compositions, (a) HA (b) HA-3 wt. % ZnO, (c) and (d) represent the variation of resistances of grain and grain boundaries with the inverse of temperature.

4.5. Antibacterial response of HA-xZnO composites

4.5.1. MTT assay

The viability of *E. coli* and *S. aureus* bacteria on unpolarized and polarized HA and HA-xZnO (x = 4.5 and 7.5 wt. %) composites are shown in Fig. 4.8 (a) and 4.8 (b), respectively.

It is observed that the viability of *E. coli* and *S. aureus* bacteria decreases significantly with addition of ZnO in HA-xZnO (x= 3, 4.5, 7.5 wt. %) composites. As far as the combined effect of ZnO addition and polarization is concerned, more pronounced

reduction in viability of both, *E. coli* and *S. aureus* has been observed on negatively and positively charged HA- 7.5 ZnO composites, respectively. These results suggest that the antibacterial response of the charged surface depends upon the charge polarity and bacteria. The population of *E. coli* and *S. aureus* bacteria are reduced by (9.62, 14, and 37.5%) and (8.69, 14.19, and 24.69 %) with the addition of ZnO in HA-x ZnO (x = 3.0, 4.5 and 7.5 wt. %) composite, respectively, as compared to HA. After polarizing the samples, viability of *E. coli* and *S. aureus* bacteria decreased by 23, 10, and 15.4, 19 %, respectively, on negatively and positively charged HA as compared to uncharged HA. The viability of *E. coli* bacteria on negatively and positively charged HA-x ZnO (x = 3.0, 4.5 and 7.5 wt. %) composites are reduced by (31.5, 43.7, 53%) and (20, 23, 41.3 %) respectively, as compared to uncharged HA. However, for *S. aureus* bacteria, negatively and positively charged surfaces of similar composition demonstrate (26, 29.6, 39.7 %), and (36, 41, 52%) reduction in viability, respectively with respect to uncharged HA. Overall, it has been observed that the combined action of ZnO addition and polarization significantly reduces the viability of *E. coli* and *S. aureus* bacteria.
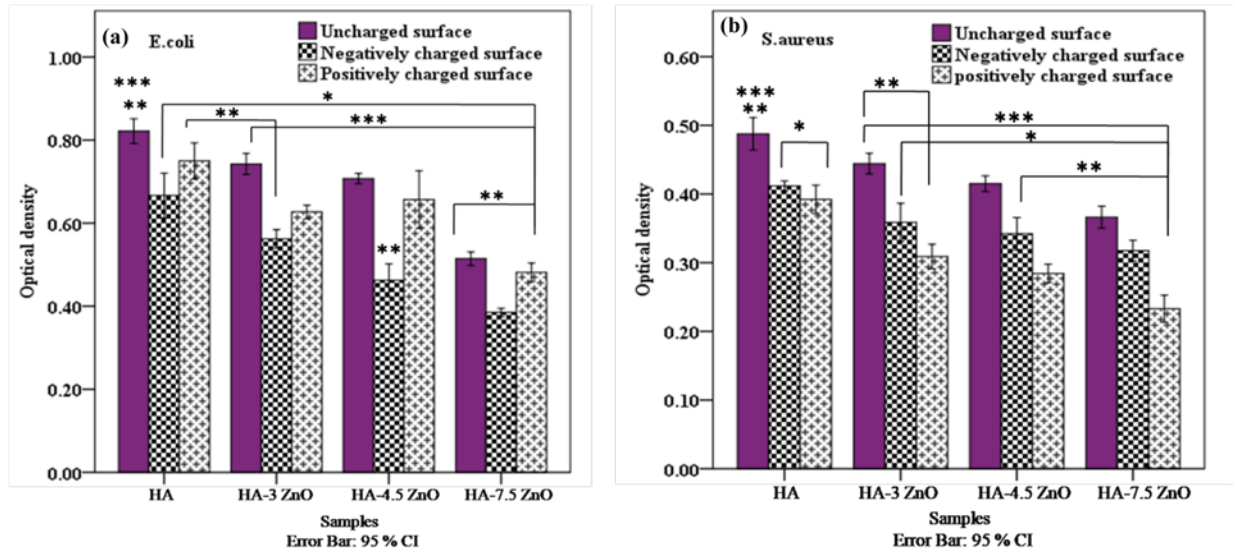
Fig. 4.8. The viability of (a) E. coli and (b) S.aureus bacteria on unpolarized and polarized HA- xZnO composites. Asterisk (*) mark represents the statistically significant difference among all samples with respect to uncharged HA at p < 0.05. Asterisk marks (**) and (***) represent the statistically significant difference among all samples with respect to negatively charged and positively charged HA, respectively, at p < 0.05.

4.5.2. Kirby-Bauer disk diffusion method

The antibacterial activity of unpolarized and polarized HA-x ZnO (x = 3, 4.5, and 7.5 wt. %) composites were also investigated using disc diffusion method. This assay was performed according to Kirby-Bauer disk diffusion method. Both, *E. coli* and *S. aureus* bacteria were cultured in agar plates. Following this, unpolarized and polarized samples were placed over the cultured agar plate and the inverted plate was incubated for 12 h at 37 ºC. The colony formation on the unpolarized and polarized surface of the samples was observed. The scrub from the area under the samples were transferred with inoculation loop to a new agar plate and further incubated for 12 h. The bacterial colonies were observed after incubation. Figs. 4.9 and 4.10 represent the results of Kirby-Bauer test for antibacterial activity of both, *E. coli* and *S. aureus* bacteria on unpolarized and polarized HA and HA- x ZnO (x = 3.0, 4.5, and 7.5 wt. %) composites, respectively. It is clearly

observed that the colony formation on agar plates for both the bacteria decreases with increasing the ZnO content in HA matrix. In addition, the polarization of samples further reduces the bacterial growth for both the bacteria. The zone of inhibition, observed under the samples, are not significantly differentiable [Figs 4.9 (e-h) and 4.10 (e-h)] and therefore, the swab under the samples was further used for striking using sterilized inoculation loop in a new agar plate to visualize the bacterial growth [Figs. 4.9 (i-l) and 4.10 (i-l)]. It is clearly observed that the bacterial growth decreases with increase in the ZnO content in HA matrix for both, *E. coli* and *S. aureus* bacteria, which further decreases after polarization treatment. It is evident that the swab under negatively charged samples has lower growth as compared to positively charged and uncharged samples for *E. coli* bacteria. However, for *S. aureus* bacteria, positively charged surface demonstrates lower bacterial growth as compared to uncharged and negatively charged samples. Overall, this result demonstrates that the growth of both the bacteria decreases remarkably with ZnO addition in HA and subsequent, polarization.
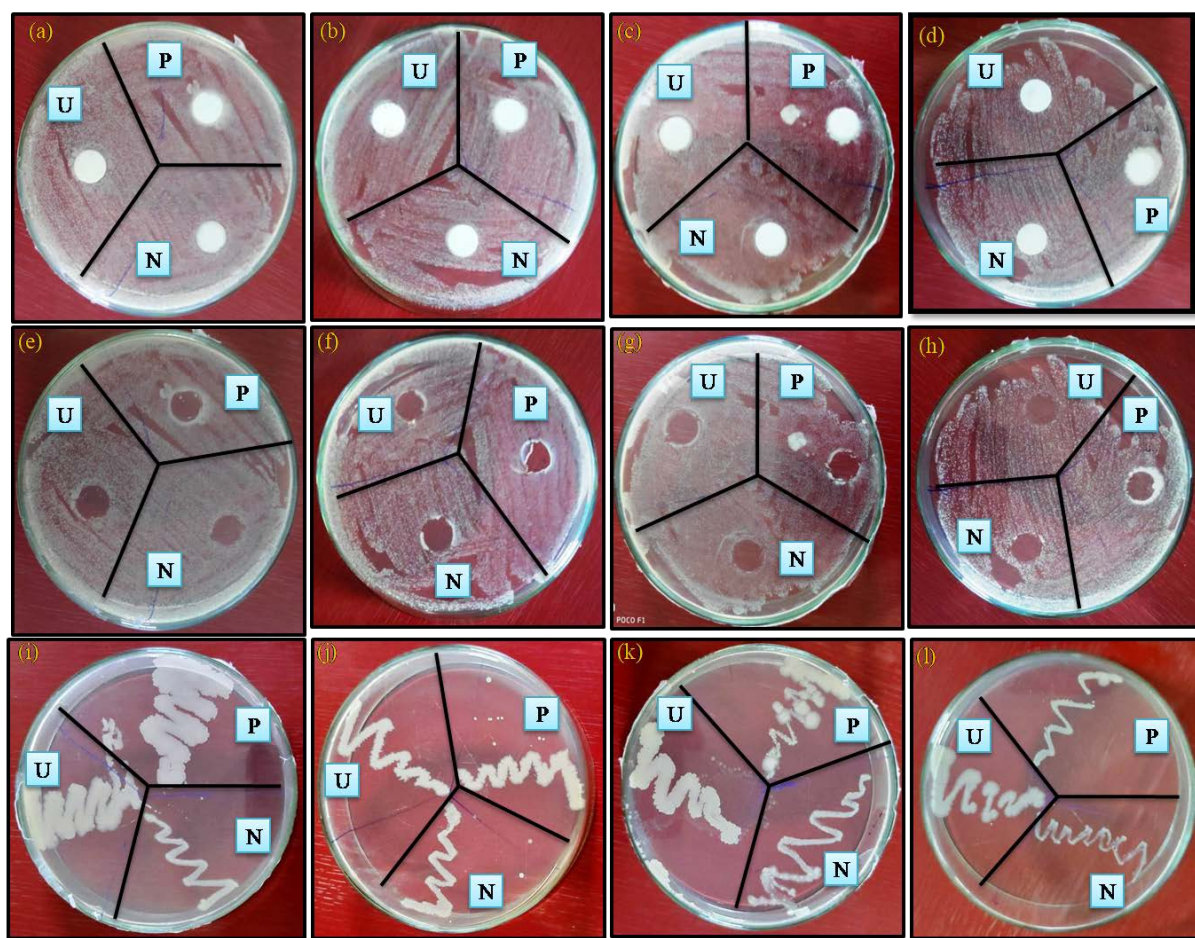
Fig. 4.9. The Kirby Bauer test performed for unpolarized (U), positively (P) and negatively (N) polarized HA-x ZnO (x = 3.0, 4.5, 7.5 wt. %) composites on agar culture plate, using E. coli bacteria, (a-d) represent the cultured agar plates, after incubation of 12 h, (e-h) area under the samples and (i-l) represent the colony formation, after transferring swab from the area under the samples on agar plates.
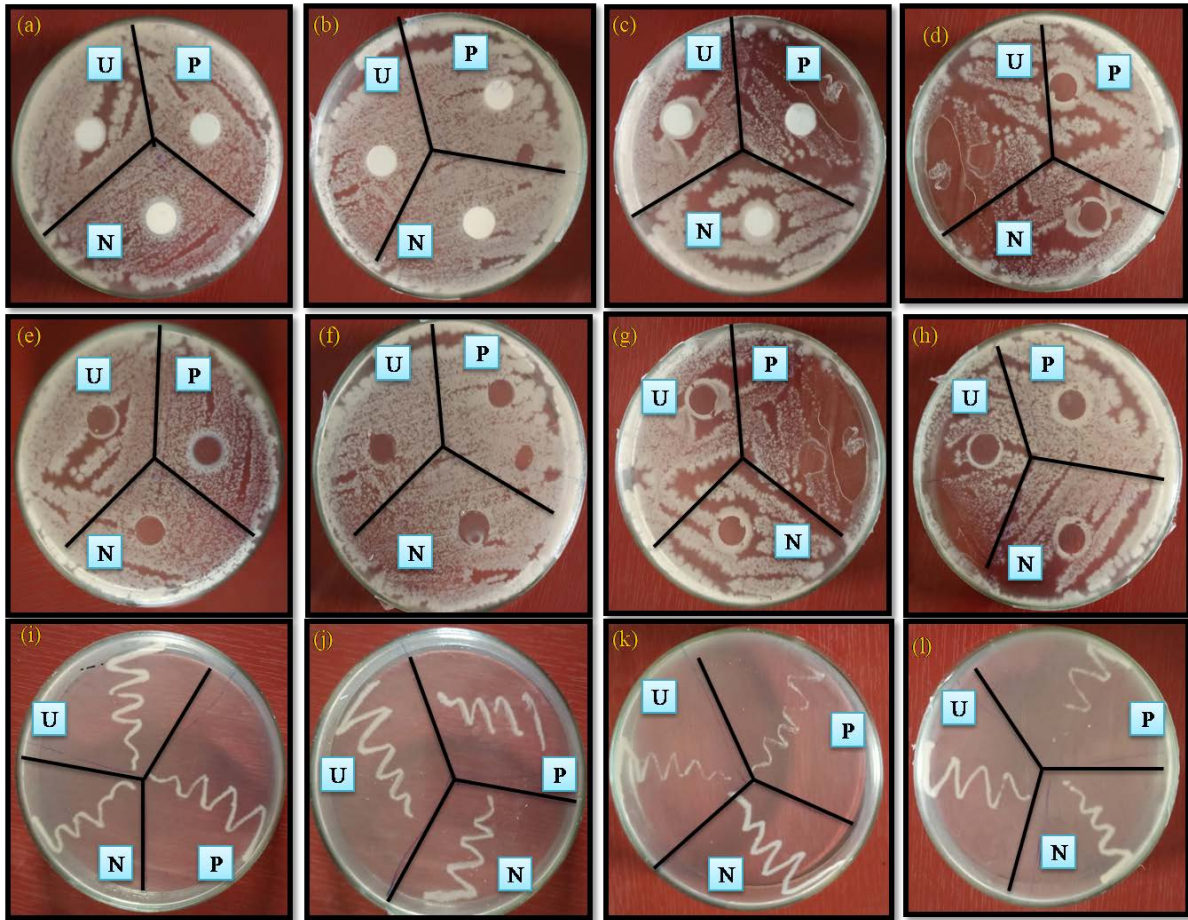
Fig. 4.10. Kirby Bauer test performed for unpolarized (U) positively (P) and negatively (N) polarized HA-x ZnO (x = 3.0, 4.5, 7.5 wt. %) composites on agar culture plate, using S. aureus bacteria, (a-d) represents the cultured agar plates, after incubation of 12 h, (e-h) area under the samples and (i-l) represent the colony formation, after transferring swab from the area under the samples on agar plates.

4.5.3. NBT assay

The NBT assay was performed to quantify the polarization induced superoxide anions (O^{2-}) production [32]. The samples were cultured with *E. coli* and *S. aureus* bacteria and after required incubation period, 300 µl of NBT solution was added in the samples and incubated further for 1 h. The O^{2-} ions dilute NBT and produce a blue color precipitate (diformazan) which was dissolved in DMSO solution [33]. The absorbance of these dissolved diformazan was taken at 595 nm, which is directly proportional to the

produced O^{2-} [36]. Figs. 4.11 (a) and (b) represent the production of O^{2-} ions in *E. coli* and *S. aureus* bacteria, cultured on unpolarized and polarized surfaces of HA and HA-x ZnO (x = 3, 4.5 and 7.5 wt. %) composites, respectively, after specific incubation period. The statistical analyses reveal that the production of O^{2-} ions on positively charged surface is significantly higher than negatively charged and uncharged surfaces. It has been reported that polarized piezoelectric sodium potassium niobate (NKN) surface produces micro electric field on its surfaces which generates ROS and kill the bacteria [79]. Overall, the NBT assay suggests that positively charged surface produces more O^{2-} ions for both, *E. coli* and *S. aureus* bacteria as compared to negatively charged and uncharged surfaces.
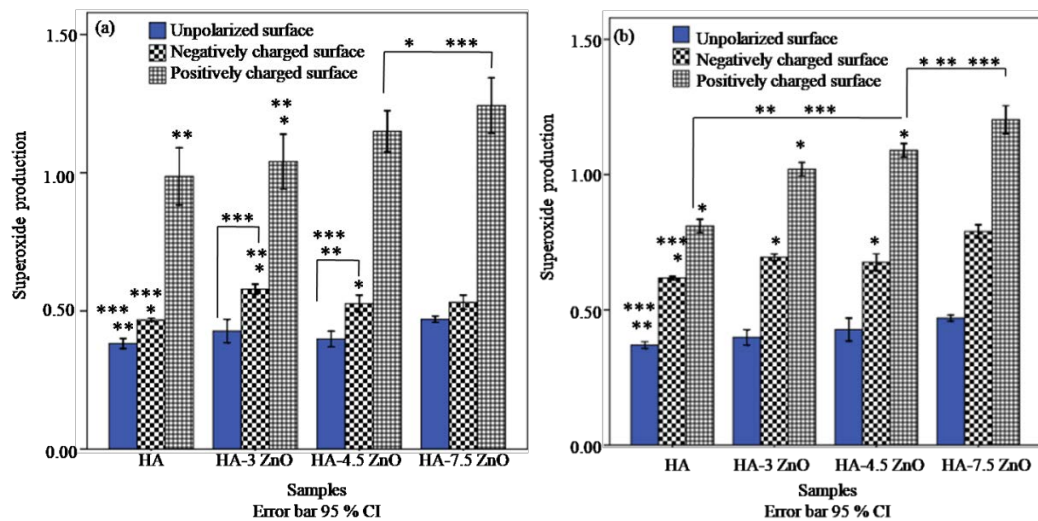

Fig. 4.11. The superoxide production in (a) E. coli and (b) S. aureus bacteria on unpolarized and polarized HA-x ZnO composites. Asterisk (*) mark represents the statistically significant difference among all samples with respect to uncharged HA, at p < 0.05. Asterisk marks (**) and (***) represent the statistically significant difference among all samples with respect to negatively charged and positively charged HA, respectively, at p < 0.05.

4.5.4. Atomic absorption spectroscopy (AAS) test

The release of Zn^{2+} ions in culture media were examined using AAS test. The samples were dipped in nutrient broth (culture media) and incubated for 12 h. After incubation, the samples were removed and the culture solution was filtered using 0.22 micron syringe filter. The filtered solution was used for AAS test. The AAS test was performed in AA7000 Shimadzu atomic absorbance spectrometer. Fig.4.12 represents the concentration of Zn^{2+} ions, released from HA-x ZnO (x = 3, 4.5, and 7.5 wt. %) composites, while immersed in culture media for 12 h. It is clearly observed the Zn^{2+} concentration increases with increasing the ZnO content in the composite. The significant enhancement in the concentration of Zn^{2+} ions is obtained among all the samples as compared to HA-3 wt. % ZnO composite [represented as (*) in Fig.4.12].

It is observed that HA-7.5 wt. % ZnO composite, released more Zn^{2+} ions as compared to both HA - x ZnO (x = 3.0, 4.5 wt.%) composites, after incubation of 12 h at 37 ℃.
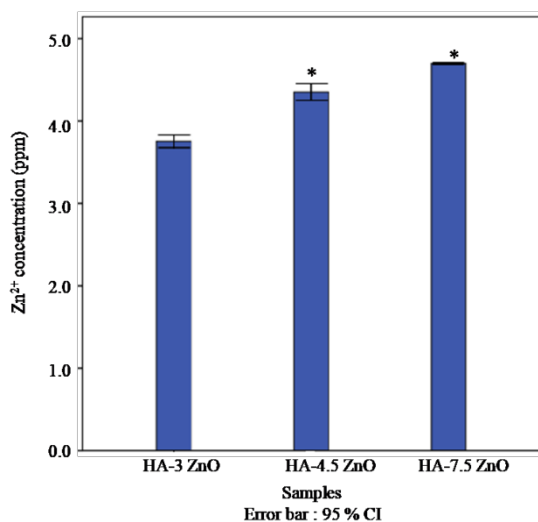

Fig. 4.12. Content of Zn^{2+} ions, released from HA-x ZnO (x = 3.0, 4.5, and 7.5 wt. %) composites in nutrient broth after incubation of 12 h. Asterisk mark (*) represents the significant difference among all samples with respect to HA -3.0 ZnO, at p < 0.05.

4.5.5 Live-dead assay

The fluorescent microscopy images for both, *E. coli* and *S. aureus* bacteria, adhered on uncharged, positively and negatively charged surfaces of HA, HA-x ZnO (x = 3.0, 4.5 and 7.5 wt. %) composites are shown in Figs. 4.13 and 4.14, respectively. The population of live bacteria decreases with increasing the ZnO content in composite for both, *E. coli* and *S. aureus* bacteria. It is observed that the adherence of *E. coli* bacteria on negatively charged surface is lower than that of positively and uncharged surfaces. However, for both the bacteria, positively charged surface demonstrate more dead bacteria as compared to uncharged and negatively charged surface (Figs. 4.13 and 4.14). It is observed that positively charged HA-7.5 ZnO composite have more dead bacterial cells for both, *E. coli* and *S. aureus* bacteria as compared to other samples. Overall, the combined action of ZnO addition and polarization in HA-x ZnO composites increases the number of dead bacterial cells for both, *E. coli* and *S. aureus* bacteria.
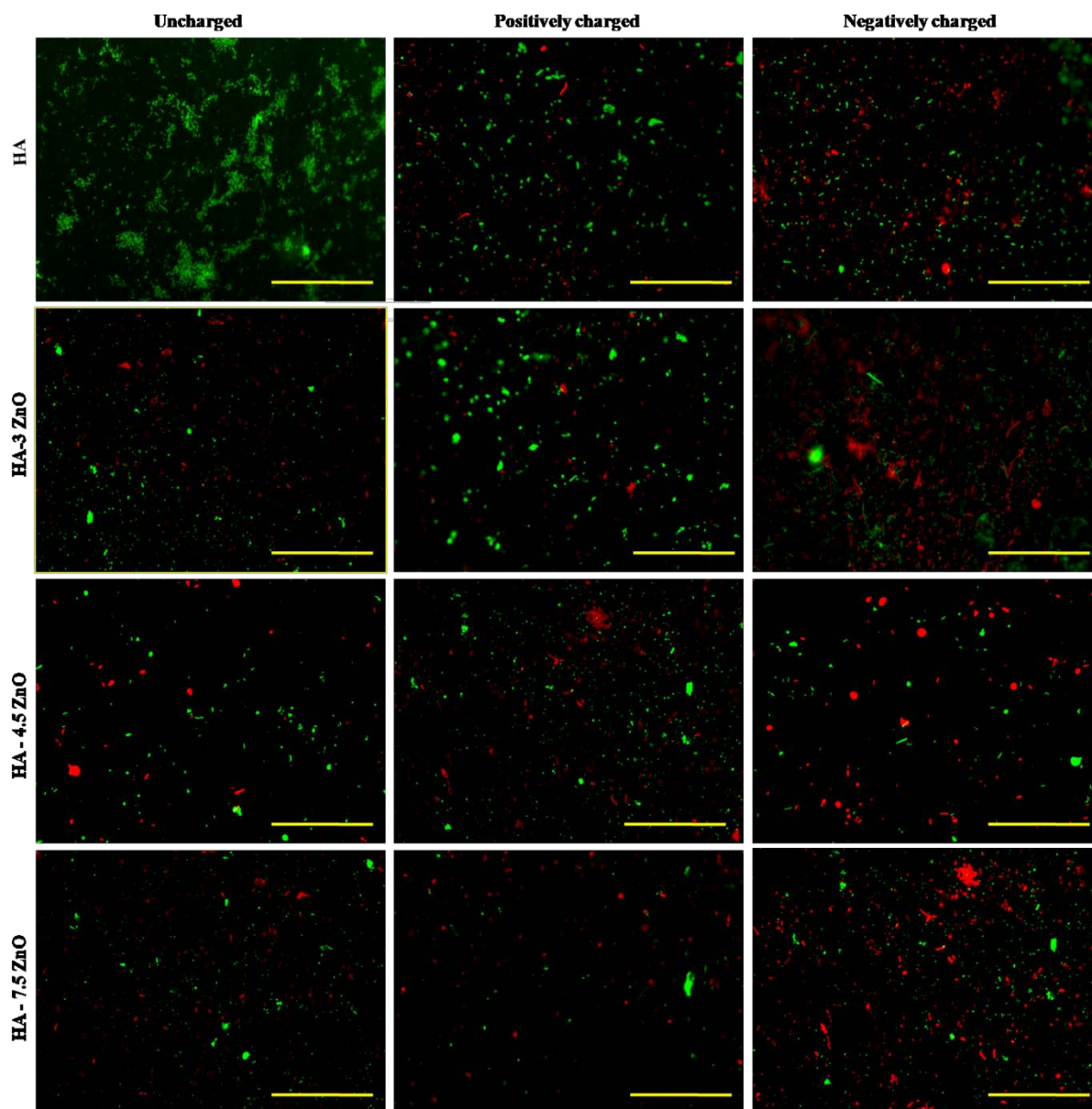
Fig. 4.13. Fluorescent microscopy images of live and dead E. coli bacteria, while cultured on uncharged, positively and negatively charged HA and HA-x ZnO (x= 3.0, 4.5 and 7.5 wt. %) composites. Live bacteria (green) are stained with SYTO 9 dye and dead bacteria (red) are stained with propidium iodide (scale bar corresponds to 100 µm).

Fig. 4.14. Fluorescent microscopy images of live and dead S.aureus bacteria, while cultured on uncharged, positively and negatively charged HA and HA-x ZnO (x = 3.0, 4.5, and 7.5 wt. %) composites. Live bacteria (green) are stained with SYTO 9 dye and dead bacteria (red) are stained with propidium iodide (scale bar corresponds to 100 µm).
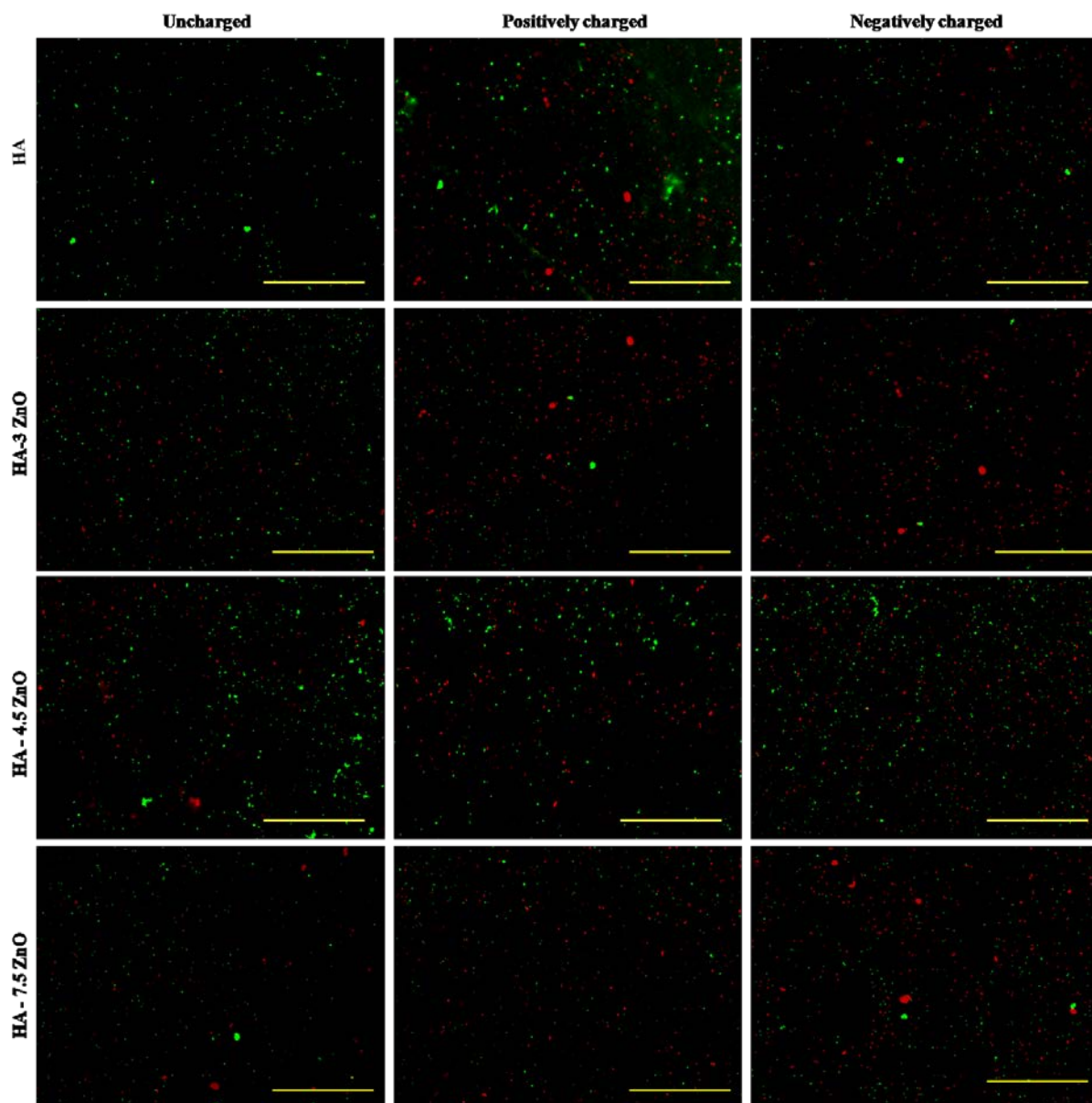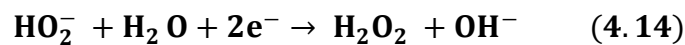
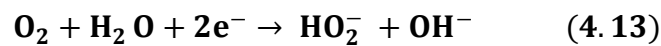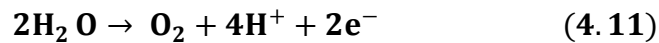It has been reported that the chemical composition and structure of outer cell wall of both, gram negative and gram-positive bacteria are different [34]. The cell wall of gram-negative bacteria has an outer layer of lipopolysaccharides [35]. However, a thick

peptidoglycan layer is present in gram positive bacteria. Gram negative bacteria have more negative charge as compared to gram positive bacteria due to the presence of lipopolysaccharides layer [36]. The zeta potential for *E. coli* and *S. aureus* bacteria has been reported to be -49 and -31.7 mV, respectively [37].The adhesion of *E. coli* bacteria on negatively charged surfaces reduce due to electrostatic repulsion [38]. In another study, it has been reported that ZnO dissolved in culture media and produces reactive oxygen species (ROS) such as OH⁻, H_2O_2, O^{2-}, and Zn^{2+} ions [39]. ROS reacts with lipid layer of the cell wall and destroys the cell structure which leads to the death of bacterial cells [40]. Zn^{2+} ions diffuse into the cell wall and damage the outer peptidoglycan layer [41]. It has been suggested that the polarization increases the hydrophilicity of surfaces, irrespective of charge polarity [42]. Such hydrophilic surfaces reduce the adhesion of bacterial cells [43]. Tan et al. [44] reported that positively charged surface promotes the ROS generation through the electrolysis reactions (Eq. 4.11- 4.14) as,

$$2H_2O \rightarrow O_2 + 4H^+ + 2e^- \qquad (4.11)$$

$$2H_2O \rightarrow OH^- + H^+ \qquad (4.12)$$

$$O_2 + H_2O + 2e^- \rightarrow HO_2^- + OH^- \qquad (4.13)$$

$$HO_2^- + H_2O + 2e^- \rightarrow H_2O_2 + OH^- \qquad (4.14)$$

It has been demonstrated that generation of ROS increases the permeability of cell which can penetrate the cell wall and disrupts the bacterial cell membranes. Fig.4.15 schematically represents the mechanism for antibacterial response on polarized HA and HA-x ZnO (x = 4.5 and 7.5 wt. %) composites, as discussed above [45].
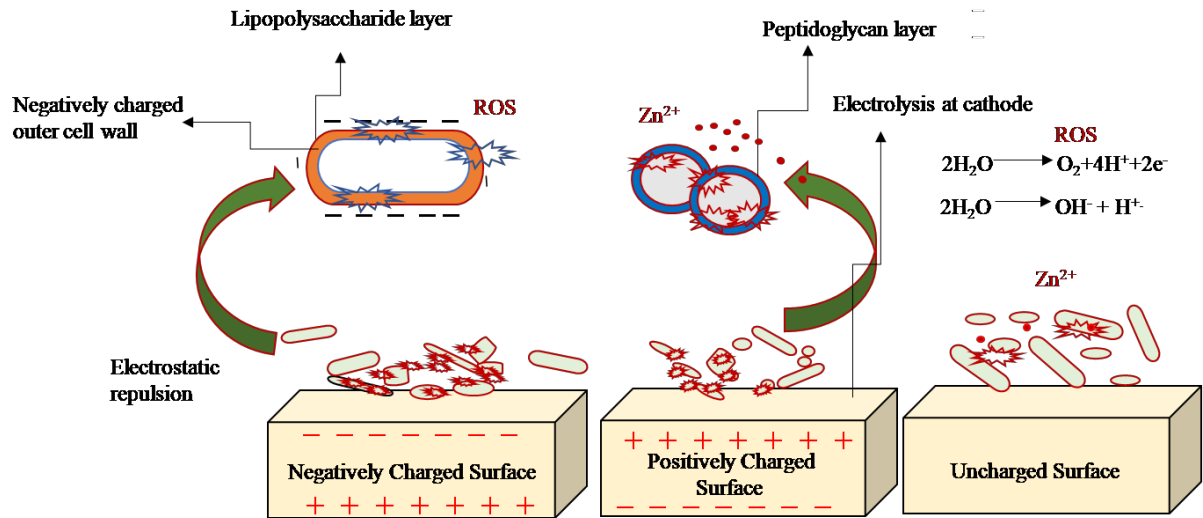
Fig. 4.15. Schematic diagram, illustrating the proposed mechanism for antibacterial response of gram positive and gram negative bacteria on polarized HA-x ZnO (x = 3.0, 4.5, 7.5 wt. %) composites.

4.6. *In-vitro* cellular response

4.6.1. MTT assay

The viability of osteoblast-like SaOS2 cells on unpolarized and polarized HA and HA-xZnO (x = 3, 4.5 and 7.5 wt. %) composites are demonstrated in Fig.4.16. The statistical analyses reveal that the viability of SaOS2 cells significantly increases with addition of ZnO in HA-x ZnO (x = 3, 4.5, and 7.5 wt. %) composites. The viability of SaOS2 cells significantly increases on all unpolarized and polarized samples after 3, 5 and 7 days of incubation as compared to uncharged HA [represented as (*) in Fig 4.16]. As far as the influence of polarization is concerned, negatively charged surface demonstrated significant enhancement in viability of SaOS2 cells with respect to uncharged and positively charged surfaces for the same sample after 3, 5 and 7 days of incubation[represented as (**) and (***) in Fig 4.16]. It has been observed that the viability of SaOS2 cells on HA-xZnO (x = 3, 4.5 and 7.5 wt. %) composites are

increased by (32, 25, 12 %), (23, 61, 41 %), and (11, 19, 28 %) with respect to HA after incubation of 3, 5 and 7 days, respectively. In contrast, the viability of SaOS2 cells on negatively and positively charged HA is increased by (31, 18, 75 %), (9, 7, 46 %) after incubation of 3, 5 and 7 days, respectively. As far as the combined effect of ZnO addition and polarization is concerned, the negatively charged HA-xZnO (x = 3, 4.5 and 7.5 wt. %) composite shows (47.2, 68, 77 %), (44.7, 74, 70%) and (70.3, 64, 62.5 %) enhancement in viability of SaOS2 cells as compared to uncharged HA after 3, 5, and 7 days of incubation, respectively. However, positively charged surfaces of similar composition demonstrate (41.4, 32, 34 %), (33, 67, 65 %) and (41, 28, 51 %) enhancement in viability of SaOS2 cells after similar incubation conditions. Overall, the negatively charged HA-x ZnO composite demonstrate the pronounced enhancement in the viability of SaOS2 cells as compared to uncharged and positively charged surfaces.
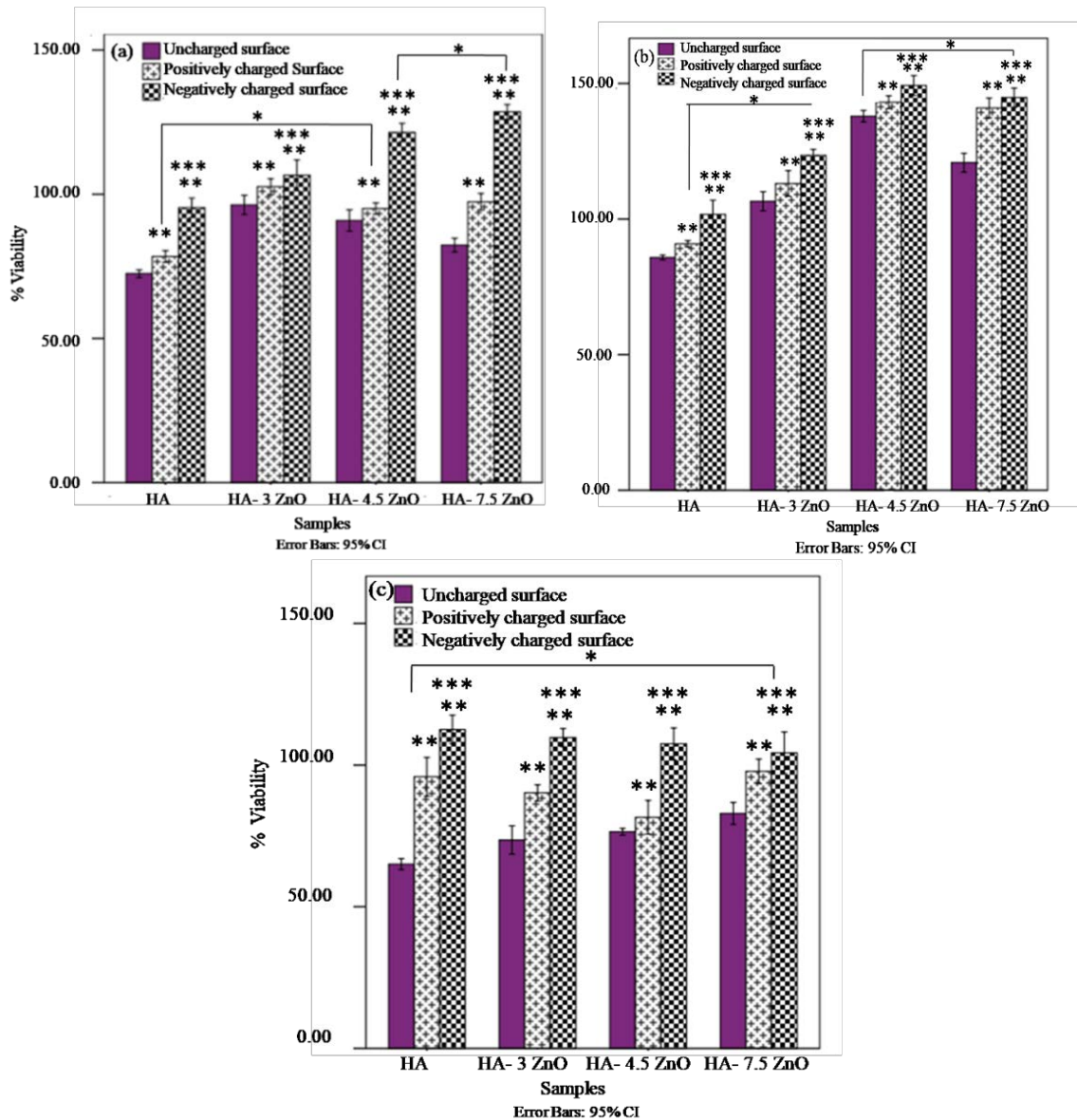
Fig. 4.16. The percentage cell viability of SaOS2 cells on unpolarized and polarized HA-xZnO (x = 3, 4.5 and 7.5 wt. %) composites after (a) 3, (b) 5 and (c) 7 days of incubation, respectively. Asterisk (*) mark represents the significant difference among all the samples with respect to uncharged HA, at p < 0.05. Asterisk marks (**) represent the statistically significant difference between polarized surfaces with respect to unpolarized surfaces for the same sample, at p < 0.05 and Asterisk (***) mark represents the statistically significant difference between negatively charged surfaces with respect to positively charged surfaces for the same sample, at p < 0.05.

4.6.2 Morphological study

Fig. 4.17 represents the fluorescent microscopy images of stained nucleus of SaOS2 cells, adhered on unpolarized and polarized HA and HA- x ZnO (x = 3, 4.5, and 7.5 wt. %) composites, after incubation of 3 days. The cell density of SaOS2 cells increases with increasing the ZnO content in HA-x ZnO (x = 3.0, 4.5, and 7.5 wt. %) composites. In addition, the negatively charged surface evident more cell density as compared to positively charged and uncharged surfaces of each composition. Overall, the combined effect of ZnO addition and polarization can be suggested to increase the proliferation of SaOS2 cells.
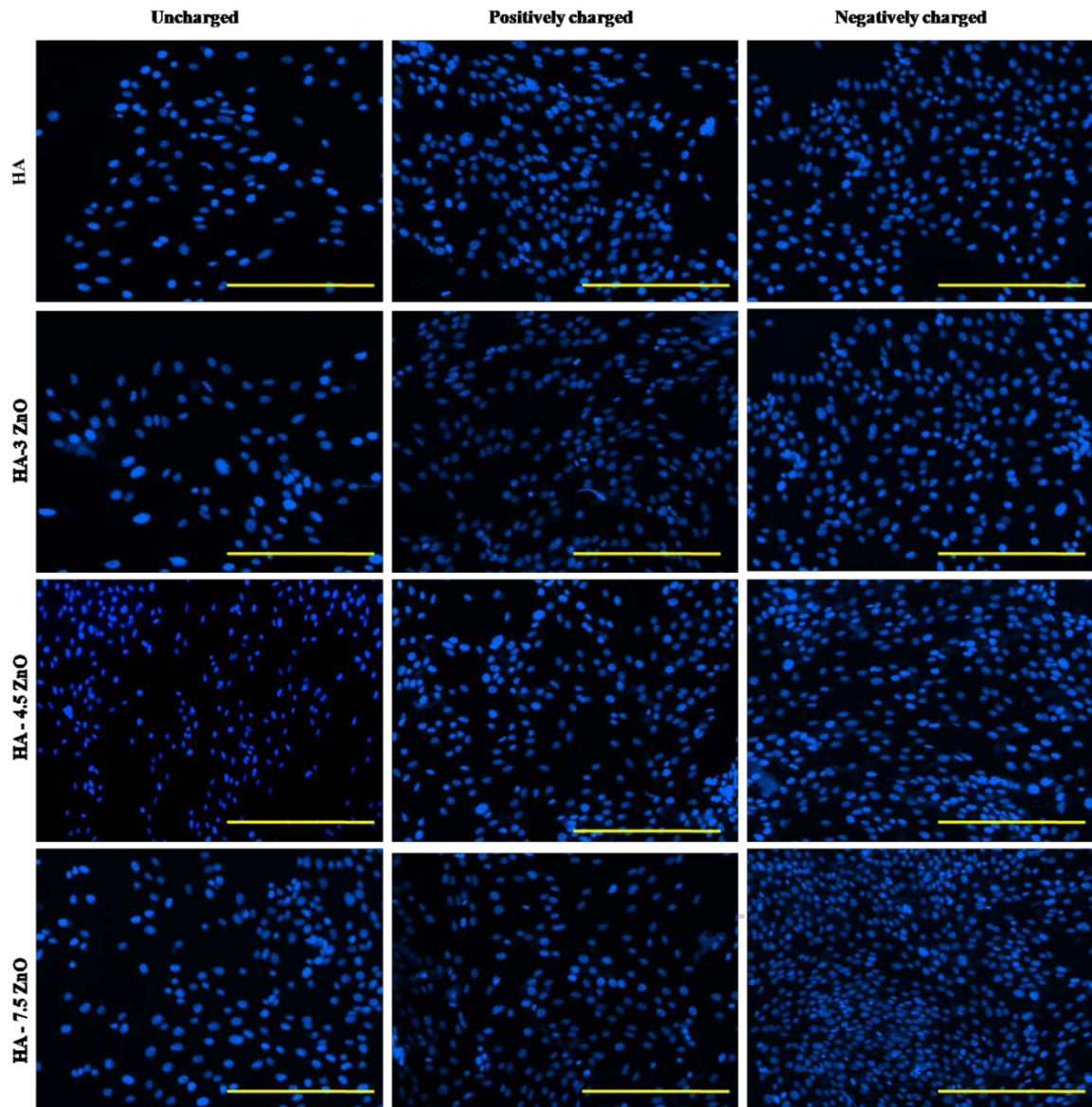
.

Fig. 4.17. Fluorescent microscopy images of SaOS2 cells (stained nucleus), adhered on uncharged, positively and negatively charged HA and HA-x ZnO (x = 3.0, 4.5 and 7.5 wt. %) composites (scale bar corresponds to 100 μm).

It has been reported that the proliferation of MC3T3-E1 osteoblast cells enhances on negatively charged HA as compared to uncharged HA, after 7 days of incubation [46,47]. Bodhak et al. [48] demonstrated that the proliferation of human osteoblast cells (hFOB) on negatively charged HA is almost doubled as compared to positively charged HA after incubation of 11 days.

The adhesion of cell with substrate depends upon the interaction between media proteins and nature of the substrate surface [49]. Selective adsorption of cations such as, Ca^+, Na^+, Mg^+ and K^+ on negatively charged surfaces attract the proteins (Fig. 4.18) and promotes the formation of bone like apatite layer which increase the cell proliferation [50,51]. In contrast, positively charged surfaces, interact with anionic groups such as, HPO_4^{2-} and HCO_3^{2-} which act as anti-adhesive agents [52]. These anions do not promote the formation of apatite layer [53].
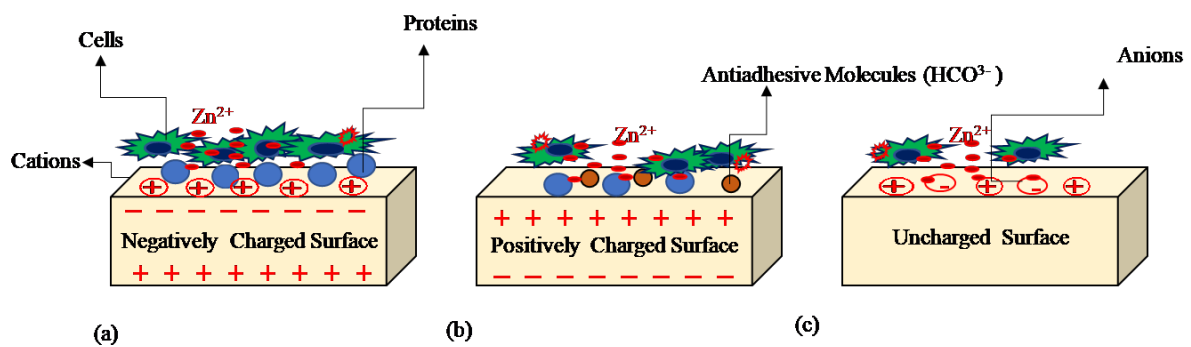

Fig. 4.18. Schematic diagram, illustrating the proliferation of SaOS2 cells on HA-x ZnO (x = 3, 4.5 and 7.5 wt. %) composite; (a) on negatively charged surface, cations interact with proteins and promote cell proliferation, (b) on positively charged surface, adhesion of anionic groups reduces cell proliferation, and (c) on unpolarized surfaces, cations and anions floats and normal cell adhesion take place.

4.7. Closure

This chapter demonstrated the successful fabrication of HA – x ZnO composite with pure phase HA and ZnO without any dissociation. The ac conductivity and dielectric constant of developed composites are measured to be almost similar to those of the natural bone. The addition of ZnO in HA matrix significantly reduces the viability of *E. coli* and *S. aureus* bacteria. The viability of *E. coli* bacteria on negatively charged HA-7.5 wt. % ZnO composite reduces by approximately 53 %. However, positively charged HA-7.5 wt. % ZnO composite shows 52 % reduction in viability of *S. aureus* bacteria. The

viability of human osteoblast-like SaOS2 cells on negatively charged HA and HA-7.5 ZnO composites increases by approximately 31.4 and 70.5 %, respectively, with respect to uncharged HA, after incubation of 7 days.

References

1. S. Raynaud, E. Champion, D. Bernache-Assollant, P. Thomas, Calcium phosphate apatites with variable Ca/P atomic ratio I. Synthesis, characterisation and thermal stability of powders, *Biomaterials*, **23** (2002) 1065–1072 https://doi.org/10.1016/S0142-9612(01)00218-6.

2. C.L. Popa, M. Albu, C. Bartha, A. Costescu, C. Luculescu, R. Trusca, S. Antohe, , Structural characterization and optical properties of hydroxyapatite/collagen matrix, *Romanian Reports in Physics*, **68** (2016) 1149–1158.

3. C Popa, C.S. Ciobanu, S.L. Iconaru, M. Stan, A. Dinischiotu, C .C. Negrila, M.M. Heino, R. Guegan, D. Predoi, Systematic investigation and in vitro biocompatibility studies on mesoporous europium doped hydroxyapatite, *Central European Journal of Chemistry* **12**(2014) (https://doi : 10.2478/s11532-014-0554-y)

4. H. Li, K.A. Khor, and P. Cheang, Effect of steam treatment during plasma spraying on the

microstructure of hydroxyapatite splats and coatings, *Journal of Thermal Spray Technology*. **15** (2006) 610-616. https://doi 10.1361/105996306X146938.

5, S. Anchez-Salcedo, M. Colilla, I. B Isabel, V. R. Maria, , Preventing Bacterial Adhesion on Scaffolds for Bone Tissue Engineering, *International journal of Bioprinting*, **2**(2015) 20−34. (https://doi 10.18063/IJB.2016.01.008).

6 N. Hitmi, E. Lamure-Plaino, A. Lamure, C. LaCabanne, R.A. Young, Reorientable electric dipoles and cooperative phenomena in human tooth enamel, *Calcified Tissue International*. **38** (1986) 252-261. https://doi 10.1007/BF02556603.

7. M.S. Kalil, H.H. Beheri, W.I.A. Fattah, Structural and electrical properties of zirconia/hydroxyapatite porous composites. *Ceramic International* **28** (2002) 451–459. https://doi.org/10.1016/S0272-8842(01)00118-3.

8. K. Yamashita, K. Kitagaki, T .Umegaki, Thermal Instability and Proton Conductivity of Ceramic Hydroxyapatite at High Temperature, *Journal of the American Ceramic Society,* **78** (2005) 119-1197.

9. N.A. Zakharov, V.P. Orlovskii, Dielectric characteristics of biocompatible $Ca_{10}(PO4)_6(OH)_2$ ceramics,*Technical Physics Letters_***27** (2001) 629–631. https://doi :10.1134/1.1398950

10. H. Suda, M. Yashima, M. Kakihana, M. Yoshimura, Monoclinic. tautm., Hexagonal Phase Transition in Hydroxyapatite Studied by X-ray Powder Di raction and Di erential Scanning Calorimeter Techniques *The Journal of Physical Chemistry A* **99** (1995) 6752-6754.(https://doi: 10.1021/j100017a068).

11. M.V. Kalinina, V.A. Moshnikov, P.A. Tikhonov, V.V. Tomaev, S.V. Mikhailichenko Temperature dependence of the resistivity for metal-oxidese miconductors based on tin dioxid, *Glass Physis and Chemistry*. **29** (2003) 422.

12. Z. Zhu, A. Chutia, R. Sahnoun, M. Koyama, H. Tsuboi, N. Hatakeyama, A. Endou, H. Takab, M. Kubo, A. Miyamoto, Theoretical study on electronic and electrical properties of nano structural ZnO *Japanese Journal of Applied Physics*. **47** (2008) 299.

13. M. Chaari, A. Matoussi, Z. Fakhfakh, Structural and dielectric properties of sintering zinc oxide bulk ceramic, *Material Science and Applications*, **2** (2011), 765-770.

14. A. Marino, R .O. Becker, and C. H. Bachman, Dielectric determination of bound water of bone. *Physics in Medicine and Biology*, **12** (1967) 367–378.

15.Y. Wu, X. Zhao, F. Li, and Z. Fan, Evaluation of mixing rules for dielectric constants of composite dielectrics by mc-fem calculation on 3d cubic lattice, *Journal of Electroceramics*, **11** (2003) 227–239.

16. R. Landauer, The electrical resistance of binary metallic mixtures, *Journal of Applied Physics,* **23** (1952) 779–784. https://doi.org/10.1063/1.1702301

17. W.D. Kingerym, H.K. Bowen, and D. R. Uhlmann, , Introduction to Ceramics, 2nd ed. New York: Wiley, (1976) 948–949.

18. O. Parkash, D. Kumar, A. Goyal, A. Agrawal, A. Mukherjee, S. Singh, and P. Singh, Electrical behaviour of zirconium doped calcium copper titanium oxide, *Journal of Physics D: applied physics,* **41** (2008), 035401.

19. G.B. Reinish, and A.S. Nowick, , Effect of Moisture on the Electrical Properties of Bone, *Journal of the Electrochemical Society,* **123** (1976) 1451-1455.

20. Zhou, X. Zhang, J. Chen, S. Zeng, K. D. Groot, High temperature characteristics of synthetic hydroxyapatite. *Journal of Materials Science: Materials in Medicine*., 4 (1993) 83–5.

21. M. Nagai, T. Nishino, Surface conduction of porous hydroxyapatite ceramics at elevated temperatures. *Solid State Ionics,* **28** (1988) 1456–61.

22. Laghzizil A, Herch N E, Bouhaouss A, Lorente G, and Macquete J, 2001 Comparison of Electrical Properties between Fluoroapatite and Hydroxyapatite Materials, J. Solid State Chem. **156**, 57-60.

23 A. Laghzizil, N.E. Herch, A. Bouhaouss, G. Lorente, and J. Macquete, Comparison of Electrical Properties between Fluoroapatite and Hydroxyapatite Materials, *Journal of Solid State Chemistry*, **156** (2001) 57-60.

24. N.A. Aal, M. Bououdina, A. Hajry, A.A. Chaudhry, J.A. Darr, A.A. Al-Ghamdi, E. H. El-Mossalamy, A.A. Al-Ghamdi, Y.K. Sung, and F. El-Tantawy, Synthesis Characterization and Electrical Properties of Hydroxyapatite Nanoparticles from Utilization of Biowaste Eggshells *Biomaterials Research,* **15** (2011) 52-59

25. R. Rani, S. Sharma, R. Rai, A,L. Kholkin, Investigation of dielectric and electrical properties of Mn doped sodium potassium niobate ceramic system using impedance spectroscopy *Journal of Applied Physics*, **110** (2011) 104102.

26. I.M. Hodge, M.D. Ingram, A.R. West, Impedance and modulus spectroscopy of polycrystalline solid electrolytes. *Journal of Electroanalytical Chemistry,* **74** (1976) 125-143.

27. J.P. Gittings, C.R. Bowen, A.C . Dent, I.G. Turner, F.R. Baxter, J.B. Chaudhuri. Electrical characterization of hydroxyapatite-based bioceramics. *Acta Biomaterialia***, 5** (2009) 743-54.

28. A.R. West, C.D. Sinclair, and N. Hirose, Characterization of Electrical Materials, Especially Ferroelectrics, by Impedance Spectroscopy, *Journal of Electroceramics*, **1** (1997) 65-71.

29. X. Guo, W. Sigle, and J. Maier, Blocking Grain Boundaries in Yttria-Doped and Undoped Ceria Ceramics of High Purity, *Journal of the American Ceramic Society,* **86** (2003) 77-87.

30. Takahashi, S. Tanase, and O. Yamamoto, Electrical conductivity of some hydroxyapatites, *Electrochimica Acta,* **23** (1978) 369-373.

31. B.S.H. Royce, Field-induced transport mechanisms in hydroxyapatite. *Annals of science* **238** (1974) 131-8.

32. H.S. Choi, J.W. Kim, Y.N. Cha, C. Kim, A quantitative nitrobluetetrazolium assay for determining intracellular superoxide anion production in phagocytic cells. *Journal of Immunoassay and Immunochemistry*, **27** (2006), 31-44.

33. M.V. Berridge, P.M. Herst, A.S. Tan, Tetrazolium dyes as tools in cell biology: New insights into their cellular reduction Biotech. *Annual Reviews*, **11** (2005) 127-152.

34. S. Shahid, S. A. Khan, W. Ahmad, U. Fatima, and S. Knawal, Size-dependent Bacterial Growth Inhibition and Antibacterial Activity of Ag-doped ZnO Nanoparticles under Different Atmospheric Conditions, *Indian Journal of Pharmaceutical Sciences,* **80** (2018) 173-180. 10.4172/pharmaceutical-sciences.1000342.

35. T. J. Beveridge, Structures of gram-negative cell walls and their derived membrane vesicles, *Journal of Bacteriology*, **181** (1999) 4725–4733.

36. R. Sonohara, N. Muramatsu, H. Ohshima, T. Kondo, Difference in surface properties between Escherichia coli and Staphylococcus aureus as revealed by electrophoretic mobility measurements. *Biophysical chemistry*, **55** (1995) 273-7.

37. E. Kłodzińska, M. Szumski, E. Dziubakiewicz, K. Hrynkiewic, E. Skware, W. Janusz, B. Buszewsk, Effect of zeta potential value on bacterial behavior during electrophoretic separation, *Electrophoresis*, **31** (2010) 1590–1596.

38. S. Kumar, R. Vaish, and S. Powar, Surface-selective bactericidal effect of poled ferroelectric materials, *Journal of Applied Physics,* **124** (2018) 014901. https://doi.org/10.1063/1.5024721.

39. W. Song, J. Zhang, J. Guo, J. Zhanga, F. Dingc, L. Li, Z. Sun, Role of the dissolved zinc ion and reactive oxygen species in cytotoxicity of ZnO nanoparticles. *Toxicology Letters,* **199** (2010) 389-397.

40. A.T. Poortinga, J. Smit, H.C. Van der Mei, J.H. Busscher, Electric Field Induced Desorption of Bacteria From a Conditioning Film Covered Substratum. *Biotechnology and Bioengineering*, **76** (2001) 395−399.

41. N. Saha, K. Keskinbora, E. Suvaci, B. Basu, Sintering, Microstructure, mechanical, and antimicrobial properties of HAp-ZnO biocomposites, *Journal of Biomedical Materials Research Part B: Applied Biomaterials*, **95B** (2010).

42. A.K. Dubey, B. Basu. Pulsed electrical stimulation and surface charge induced cell growth on multistage spark plasma sintered hydroxyapatite barium titanate piezobiocomposite *Journal of the American Ceramic Society*, **97** (2014) 481–489.

43. K. Yamashita, N. Oikawa, T. Umegaki, Acceleration and Deceleration of Bone-Like Crystal Growth on Ceramic Hydroxyapatite by Electric Poling. *Chemistry of Materials*, **8** (1996) 2697−2700.

44. G. Tan, S. Wang, Ye. Zhu, L. Zhou, Yu. Peng, X. Wang, He. Tianrui, C. Junqi, C. Mao, and C. Ning, Surface-Selective Preferential Production of Reactive Oxygen Species on Piezoelectric Ceramics for Bacterial Killing, *ACS Applied Materials & Interfaces,* **8** (2016) 24306–24309.

45. A. Singh, and A.K. Dubey, Various Biomaterials and Techniques for Improving Antibacterial Response, ACS Applied biomaterials. **1**(2018), 3−20.

46. M. Ohgaki, T. Kizuki, M. Katsura, and K. Yamashita, Manipulation of selective cell adhesion and growth by surface charges of electrically polarized hydroxyapatite, *Journal of Biomedical Materials Research Part B: Applied Biomaterials*, **57** (2001) 366-373.

47. D. Kumar, J.P. Gittings, I.G. Turner, C.R. Bowen, A. Bastida-Hidalgo, S.H. Cartmell, Polarization of hydroxyapatite: Influence on osteoblast cell proliferation, *Acta Biomaterialia*, **6** (2010) 1549–1554.

48. S. Bodhak, S. Bose, A. Bandyopadhyay, Role of surface charge and wettability on early stage mineralization and bone cell–materials interactions of polarized hydroxyapatite. *Acta Biomaterialia*, **5** (2009) 2178–2188.

49. F. Grinnell, and M.K/ Feld, Fibronectin adsorption on hydrophilic and hydrophobic surfaces detected by antibody binding and analyzed during cell adhesion in serum-containing medium, *Journal of Biological Chemistry,* **257** (1981), 4888-1982.

50. E.G. Hayman, M.D. Pierschbacher, S. Suzuki, and E. Ruoslahti, Vitronectin a major cell attachment-promoting protein in fetal bovine serum. *Experimental Cell Research*, **160** (1985) 245-258.

51. W. Chen, Yu. Zunxiong, J. Pang, Yu. Peng, T. Guoxin, and C. Ning, Fabrication of Biocompatible Potassium Sodium Niobate Piezoelectric Ceramic as an Electroactive Implant, *Materials*, **10**, (2017) 345.

52. C.J. Wilson, R.E. Clegg, D.I. Leavesley, M.J. Pearcy, Mediation of biomaterial-cell interactions by adsorbed proteins: A review. *Tissue Engineering*. **11** (2005) 1–18.

53. C. Yoshida-Noro, N. Suzuki, M. Takeichi, Molecular nature of the calcium-dependent cell-cell adhesion system in mouse teratocarcinoma and embryonic cells studied with a monoclonal antibody. *Developmental. Biology*. **101** (1984) 19–27.